Samyn P,[1] Van Schepdael L,[2] Leendertz JS,[3] Van Paepegem W,[4] De Baets P,[5] Degrieck J[6]

Short-beam-shear testing of carbon fibre/epoxy ring segments with variable cross-sectional geometry as a representative selection criterion for full-scale delamination

ABSTRACT : Carbon fibre reinforced/epoxy (CFR-E) rings are used as radial reinforcement for polyethylene bearing elements with diameter 249 mm, functioning under 150 MPa. Full-scale static and dynamic testing revealed circumferential splitting of carbon fibres near the top of the ring, unfavourable for counterface wear during sliding. As full-scale tests are however expensive and time-consuming, a representative short-beam-shear test is designed for determination of the interlaminar shear strength of the composite ring. A standard sample geometry could however not be applied as the reinforcing ring contains machined edges contributing to stress concentrations. A full ring cross section should therefore be tested with practical implications on the applied span and supporting method. Finite element modeling is used for verification of the effects of various testing parameters on the stress distribution over the beam, such as cross-section geometry, beam curvature and convex/concave loading. It is concluded that full-scale fracture depends on a non-hydrostatic stress state near the machined ring edge and a 27 kN equivalent normal load is required on small-scale short-beam-shear for avoiding fracture.

KEYWORDS : full-scale, small-scale, finite elements, composite, shear

Introduction

The interlaminar shear strength (ILSS) is one of the most important parameters in determining the ability of a composite to resist delamination damage. An accurate prediction of its value, therefore, is important and a number of tests have been developed for evaluation. Standardized test methods are the three-point-bending tests according to ASTM Test Method for Apparent Interlaminar Shear Strength of Parallel Fibre Composites by Short-Beam-Shear (D 2344-00). However, concerns arise about this test because of a non-uniform bending moment along the shear plane and strong localized damage occurring underneath the loading rollers. Classical beam theory is usually used to interpret the experimental results: for a beam of rectangular cross-section, the maximum interlaminar shear stress in the mid-thickness of the beam is given by formula (1):

$$\tau = \frac{3}{4}\frac{F_N}{wt} \quad (1)$$

[1*]Research Assistant, Ghent University, St. Pietersnieuwstraat 41, B-9000 Gent, Belgium
[2]Design Engineer, Solico BV, Solutions in Composites, Everdenberg 97, NL-4902 TT Oosterhout, The Netherlands
[3]Senior Design Engineer, Ministry of Transport, Public Works and Water Management, Directorate-General,Herman Gorterhove 4, NL-2700 AB Zoetermeer, The Netherlands
[4]Professor, Ghent University, St. Pietersnieuwstraat 41, B-9000 Gent, Belgium
[5]Professor, Ghent University, St. Pietersnieuwstraat 41, B-9000 Gent, Belgium
[6]Professor, Ghent University, St. Pietersnieuwstraat 41, B-9000 Gent, Belgium
[*]*Author to whom correspondence should be addressed: Pieter.Samyn@UGent.be*

where F_N is the force applied by the loading cylinder and w and t are the width and thickness of the beam, respectively. However, for small span-to-thickness ratios, classical beam theory becomes invalid. Theoretical analysis has shown that the maximum shear stress is not constant along the beam length and the stress distributions through the thickness of the beam near the loading and supporting points were found to be skewed towards the surfaces of the beam, instead of being parabolic [1].

Other tests include the Iosipescu test (ASTM D 5379-98), the tensile test (ASTM D 3518-94) and the double notch compression test (ASTM D 3846-94). A compression test generally leads to lower shear strength as the failure consistently occurs in a well-defined single shear plane [2], yielding a rather conservative estimate for safety design.

Related to practical design of composite carbon fibre/epoxy (CFR-E) reinforcing rings as a radial reinforcement for ultra-high-molecular-weight polyethylene (UHMWPE) bearing elements (Fig. 1), full-scale compressive and sliding tests were performed during design of the ring geometry and tuning of the composite composition. The ring geometry is specifically designed with a non-parallel top and bottom surface to allow plastic flow of the UHMWPE part on top of the reinforcing ring. As such, direct contact between the ring and the counterface is avoided, as it was demonstrated this was the reason for severe counterface wear under sliding [3]. Appropriate fillets were introduced in contact with the central UHMWPE part and at the outer diameter on top of the ring. A small-scale selection test for measuring the ILSS of the entire CFR-E ring should be designed, taking into account the effects of the real specimen geometry. As the ASTM D 2344-00 standard prescribes a rectangular cross-section, it can be guessed that a machined or round edged geometry introduces additional stress concentrations during short-beam-shear testing, influencing the apparent ILSS. In contrast to previous mentioned testing methods, a “component test” is presently needed for evaluation of the shear strength of the ring geometry and selection criteria should be related to a full-scale test. This paper is part of an international test program between the Nederlandse Rijkswaterstaat, Solico (Solutions in Composites) and Ghent University (Laboratory Soete), partners involved in the re-design of the sliding surfaces of the Maeslant storm surge barrier near Rotterdam [4].

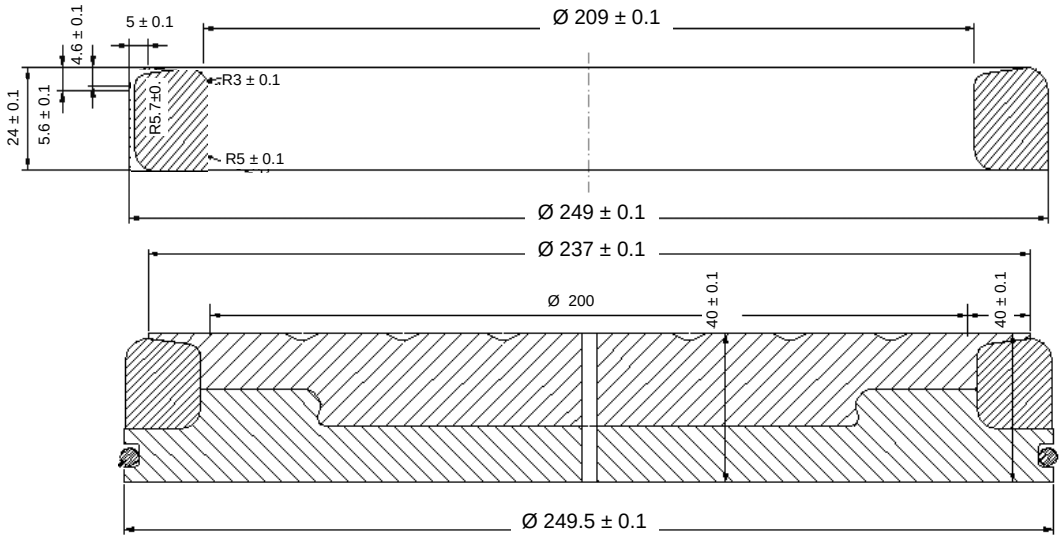

FIG. 1 — *Full-scale polymer bearing element with carbon fibre/epoxy reinforcement*

Test Material

The full-scale CFR-E ring has a nominal outer diameter of 249 mm and is made of unidirectional carbon fibre Toray T700 12K (1.8 g/cm^3) and epoxy Bakelite EPR-LB20 HXS resin with EPH 960 hardener (1.09 g/cm^3). The nominal radial thickness is 20 mm with 24 mm axial height. A filament winding process is applied over a steel mandrel with radius 104.5 mm and winding angle 90° (the rings are afterwards machined), as Liu et al. [5] compared 45, 60 and 90° winding for E-glass fibre / epoxy radial reinforcements on concrete cylinders, concluding that a 90° reinforcement has highest axial compressive strength and a 45° lowest strength. Combinations with layer sequences along various winding angles have intermediate strength. The material is transversally isotropic as it is only fibre-reinforced in the hoop winding direction, with elasticity constants E_y = 150 GPa (fibre direction) and $E_z = E_x$ = 9 GPa; Poisson coefficients $\nu_{xy} = \nu_{yz}$ = 0.34 and ν_{xz} = 0.5 and shear moduli $G_{xy} = G_{yz}$ = 4 GPa and G_{xz} = 3 GPa (notation explained in Fig. 4). Present rings have a fibre content of 60 to 63 % and porosity content < 2.5 %. Its thermal properties are determined from a DSC-test with T_G > 95°C and from a DMTA-test with T_G > 105°C. The curing times and temperatures were strictly controlled at 16 hrs room temperature, 8 to 10 hours at 60°C and 8 to 10 hours at 120°C with 15°C per hour temperature raise. The resulting tensile stress in fibre direction is 2450 MPa.

Test set-up

As the CFR-E ring acts as a reinforcement for UHMWPE bearing elements with thickness 40 mm and diameter 249 mm, a full-scale compressive test on a bearing element is performed with a convex curved counterface for validation of the ring strength and simulation of the stress distribution under working conditions of 150 MPa normal contact pressure. Therefore, a vertical hydraulic press with 10 000 kN maximum capacity is used with the reinforced UHMWPE elements retained into a steel sample holder.

Small-scale short-beam-shear tests (*SBS-tests*) are performed on CFR-E ring segments with different geometries according to Fig. 2. The ASTM D 2344 standard for testing carbon fibre composites requires a span-to-thickness ratio of 4.0 and a length-to-thickness ratio of 6.0. This standard geometry is used on a specimen of length 40 mm in Test A with a span 24 mm, a loading pin of radius 3 mm and cylindrical supports. The effect of either roller or flat supports and the beam curvature is compared in Test B1 and Test B2. Two types of rectangular sections are applied in Test C and Test D with a section 15 mm x 17 mm or 20 mm x 30 mm respectively. The original span is increased from 24 mm to respectively 60 mm and 80 mm, according to ASTM D 2344 standards. Due to practical problems attributed to high deflection however, the initial cylindrical supports are replaced by flat supports. The real ring cross-sectional geometry with machined edges is manufactured from a beam section of Test D and is evaluated in Test E applying a span of 80 mm, respecting the span-to-thickness ratio of 4.0. For a more homogeneous stress introduction on thick beams, a pin of radius 5 mm is used.

Finite element analysis is performed with EMRC-NISA software in order to determine the stresses in the CFR-E ring under full-scale loading and to give insight in the stress concentrations on different small-scale CFR-E beams, implied by the characteristic sample geometry and type of loading support. It is used to validate the state of stress in a short beam shear test to be in accordance with a full-scale test.

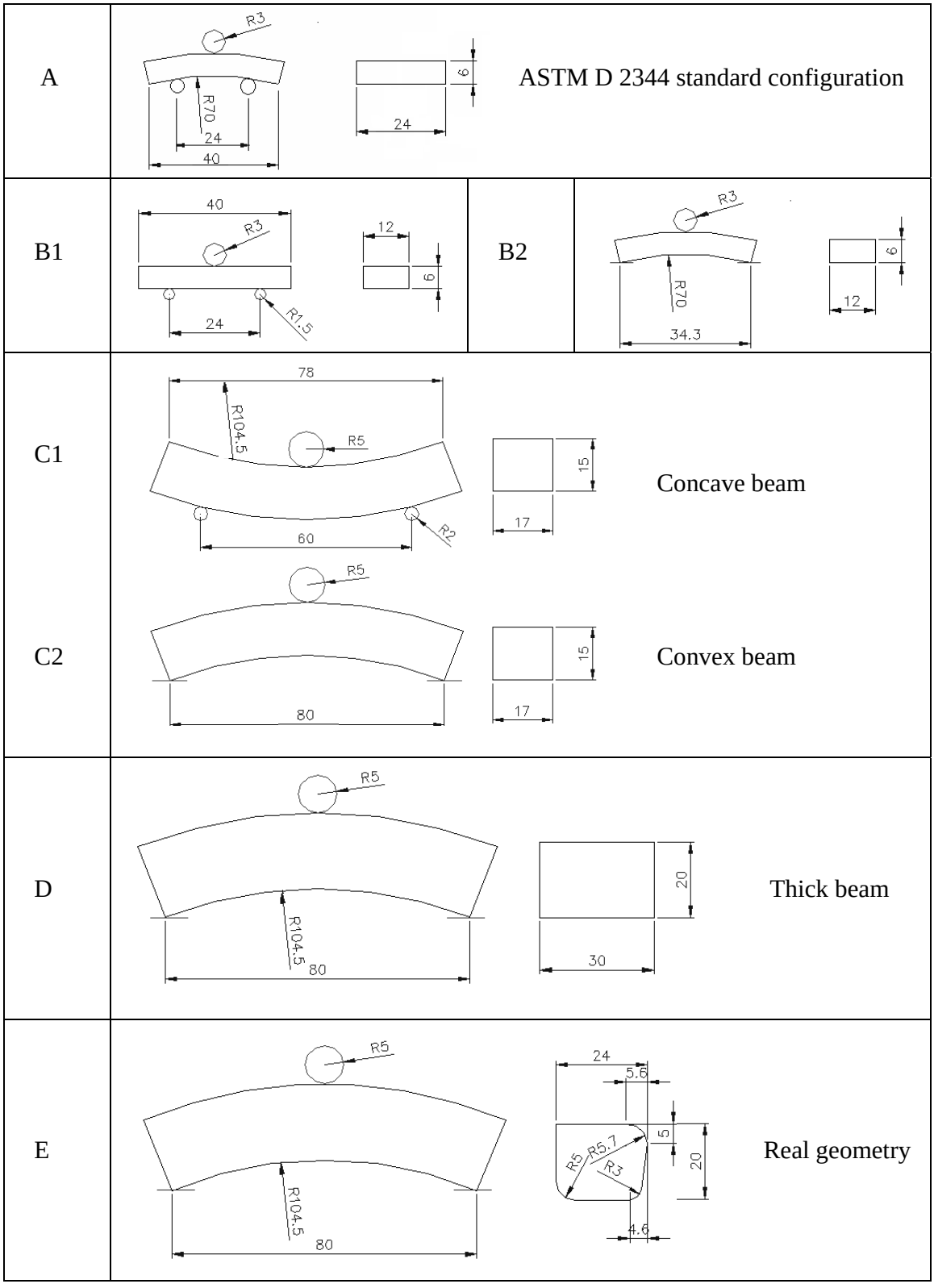

FIG. 2 — *Different sample geometries used for small-scale Short-beam-shear testing*

Full-scale test results

A cross-sectional view of damage on the CFR-E ring with real geometry after full-scale loading of a bearing element under 150 MPa compressive contact pressure is shown in Fig. 3. It is characterised by shear failure initiating at the machined edge and propagation through the bulk under 45°, with circumferential splitting of carbon fibres at the top of the machined edge. Although catastrophic failure in radial direction due to fibre breaking was not observed, shear failure is not allowed through the detrimental effects of contact between the loose carbon fibres and the sliding counterface [6]. The permanent deformation of the carbon ring is between 0.07 mm and 0.17 mm, showing that it bears the deformation implied by high tangential and radial stresses.

The CFR-E ring must withstand high *tensile hoop* stresses σ_{YY} (along the fibre direction), *radial compressive* stresses σ_{XX} (transverse to fibre direction) and *axial compressive* stress σ_{ZZ}. The safety factor on fibre fracture is larger than 2.0: the maximum stress σ_{YY} = 1094 MPa, while the ultimate tensile stress is above 2450 MPa.

The *radial-axial* shear stress τ_{XZ} under 45° relatively to the loading direction is calculated by a 3D finite element simulation (axial load F_z = -8000 kN and shear load F_X = 500 kN) in Fig. 3 and attains 33 MPa at the outer diameter towards 45 MPa immediately beneath the machined edge (under *non-hydrostatic* stress conditions), while it rises to 104 MPa in the bulk of the ring (under *hydrostatic* stress conditions). It seems that the former stress state is the most critical for full-scale shear fracture, as it is known from literature [7] that a hydrostatic stress has favourable effect on the material's strength with less tendency of fracture. The non-hydrostatic stress components at the machined edge of the CFR-E ring rise to 21 MPa (radial stress σ_{XX}) and 13 MPa (axial stress σ_{ZZ}). Both positive values indicate tensile stress components that imply a reduction in the ultimate shear stress. In the bulk of the CFR-E ring σ_{XX} = -140 to -190 MPa and σ_{ZZ} = -147 to -280 MPa, while also the hoop stress σ_{YY} becomes more negative due to the retaining action of the steel sample holder.

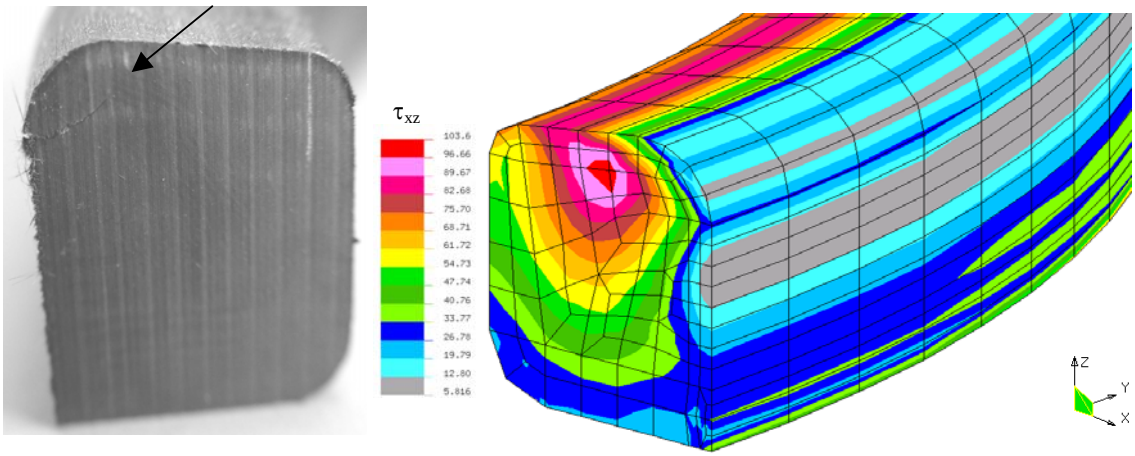

FIG. 3 — *Full-scale ring damage and shear stress analysis at 150 MPa (Solico BV)*

Small-scale test results

Finite element simulation

Model — The *SBS-tests* are linearly modelled on a quarter of the beam with two symmetrical planes, i.e. at the central loading point and at half-thickness. A comparison between linear and non-linear finite element analysis on SBS specimens demonstrated that the difference in stress is small (< 4%) [8]. A mesh as illustrated in Fig. 4 is used with more detailed nodes near the supporting points. The normal load is applied along the X-axis with a pin of appropriate radius, the Y-axis is parallel to the fibre direction and the Z-axis represents the sample thickness. The stress distribution will be studied in different cuts along the radial direction (X-axis) and at different thicknesses (Z-axis) perpendicular to the loading pin. Consequently, σ_{XX} corresponds to the radial compressive stress in full-scale tests, σ_{YY} is the tensile hoop and σ_{ZZ} corresponds to the axial compressive stresses. The *radial-tangential* shear stress τ_{XY} or ILSS is determined as 'representative' stress for radial-axial shear stress τ_{XZ}, as small-scale compression tests measuring τ_{XZ} were unsuitable. It was experimentally verified that τ_{XY} is lower than τ_{XZ} [9]. A design factor of 1.3 from experimental experience is applied on full-scale shear failure considering the maximum shear stress of 45 MPa under non-hydrostatic conditions: consequently, a critical ILSS = 58.8 MPa is required as qualification value from short-beam shear tests.

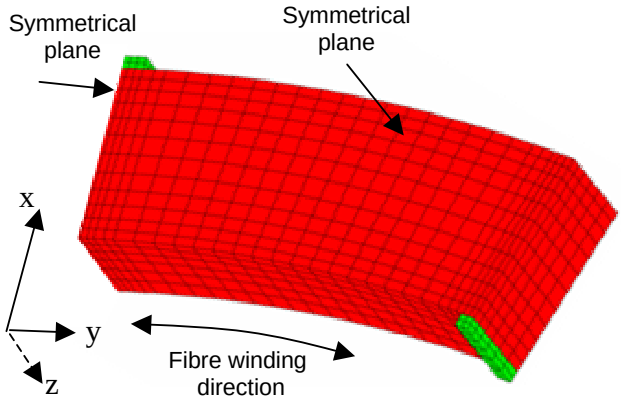

FIG. 4 — *Finite element model of a quarter beam for stress calculations (Solico BV)*

Effect of 2D and 3D Modelling on Standard Specimen Geometry — For *SBS-test* geometries B1 and B2, a normal load of 5.65 kN according to formula (1) is required as selection criterion for failure on a sample geometry with thickness 6 mm and width 12 mm. For a flat CFR-E sample with cylindrical supports (Test B1) the contact elements in the beam are either two-dimensionally, either three-dimensionally modelled and the respective stress distributions are illustrated in Fig. 5. High compressive radial stresses σ_{XX} are calculated near the supporting points, rising towards -400 MPa (blue zone) with corresponding shear stress τ_{XY} = 260 MPa. As these hydrostatic stress conditions are not relevant for full-scale shear failure, they will not be further treated. The centre of the beam with σ_{XX} close to zero is more relevant and the local shear stress τ_{XY} equals 55 MPa according to 2D modelling and τ_{XY} equals 58 MPa according to 3D modelling with better symmetry over the thickness. The implementation of a 3D stress model involves ± 5 % difference and nearly perfect agreement to the estimated ILSS from formula (1).

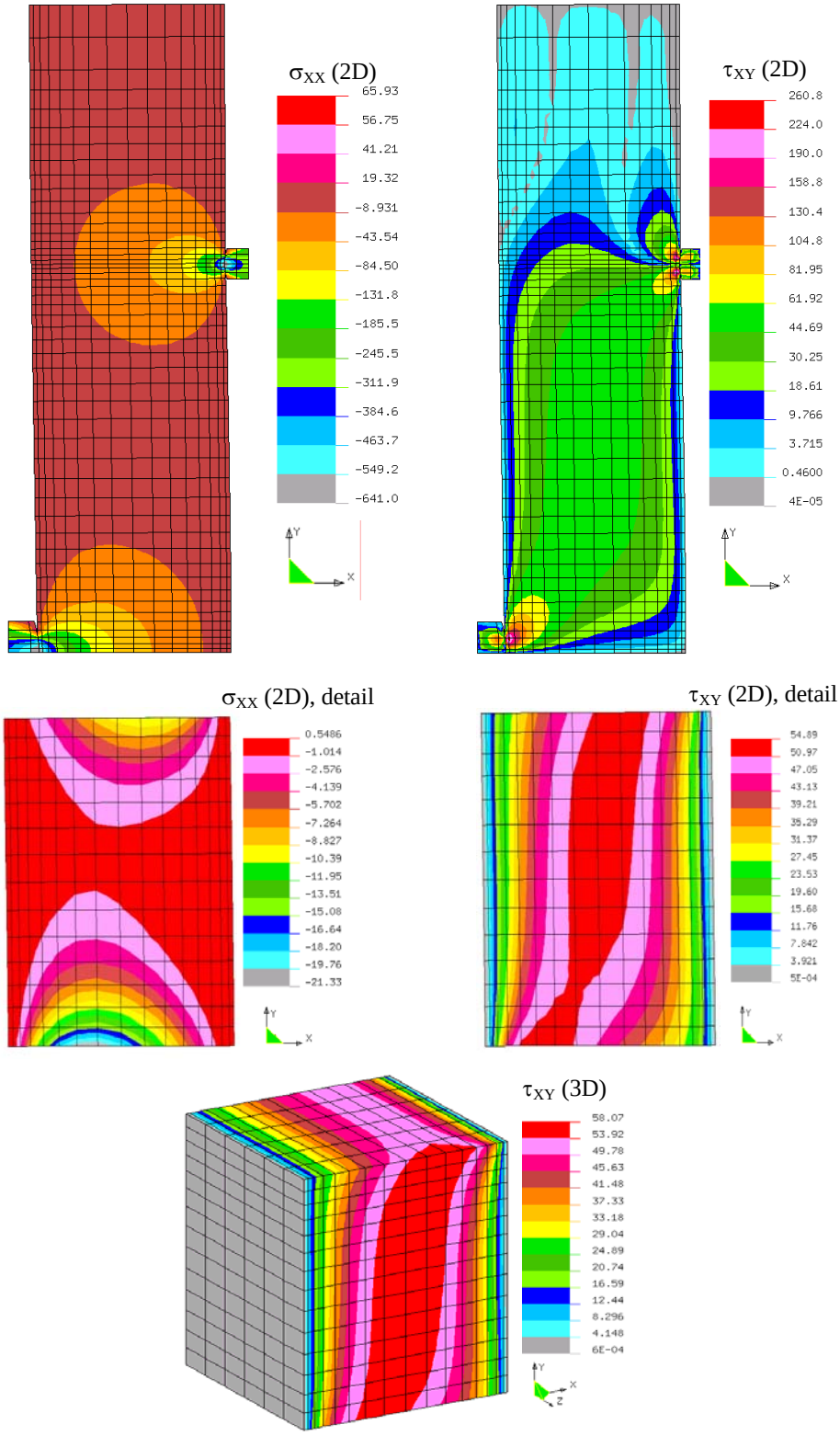

FIG. 5 — *Effect of 2D or 3D modeling of a flat sample geometry on the stress distribution according to 'Test B1' under 5.65 kN normal load (Solico BV)*

Effect of Beam Curvature on Standard Specimen Geometry — A CFR-E beam with inner radius 70 mm according to ASTM requirements and span 34 mm is loaded in a *SBS-test* (Test B2), however using flat supports rather than the prescribed cylinder supports compared to Test B1. Flat supports are presently used in relation to the finally aimed test geometry that has a large span of 80 mm and which is practically not suitable for roller supports. In practice, the flat supports have a fillet radius of 2 mm although the beam rests on the slightly declined top surface of the supports, allowing for free expansion under loading. It is clear from the stress distribution in a quarter beam segment between the loading pin and the supports as calculated in Fig. 6, that stresses are less symmetrical compared to a flat beam with cylindrical supports, either over the beam thickness and beam length: the maximum shear stresses are shifted towards the concave part of the beam and only occur beneath the loading pin. In this central part, the shear stress maximum ranges between 60 MPa and 65 MPa, while it levels towards 57 MPa in the direction of the outer supporting points. Also stress concentrations near the loading supports are lower compared to the situation in Fig. 5 for roller supports. Compared to the ASTM estimation from Formula (1) a slightly higher maximum shear stress is however calculated from finite element analysis caused by the larger deflection of the curved beam geometry and the applied flat supports. The radial compressive stresses σ_{XX} for a curved CFR-E segment are negative near the supporting points attaining -10 MPa, although they are smaller compared to the flat CFR-E beam. The σ_{XX} stress becomes positive in the centre of the beam in contrast to nearly zero radial stress for flat specimens. These differences in stress state explain the variations in calculated shear stress between flat and curved sample geometries. Present situation in Test B2 compared to Test B1 is in better agreement to the full-scale simulation in Fig. 3 with a positive stress state in the critical zone around the machined edge.

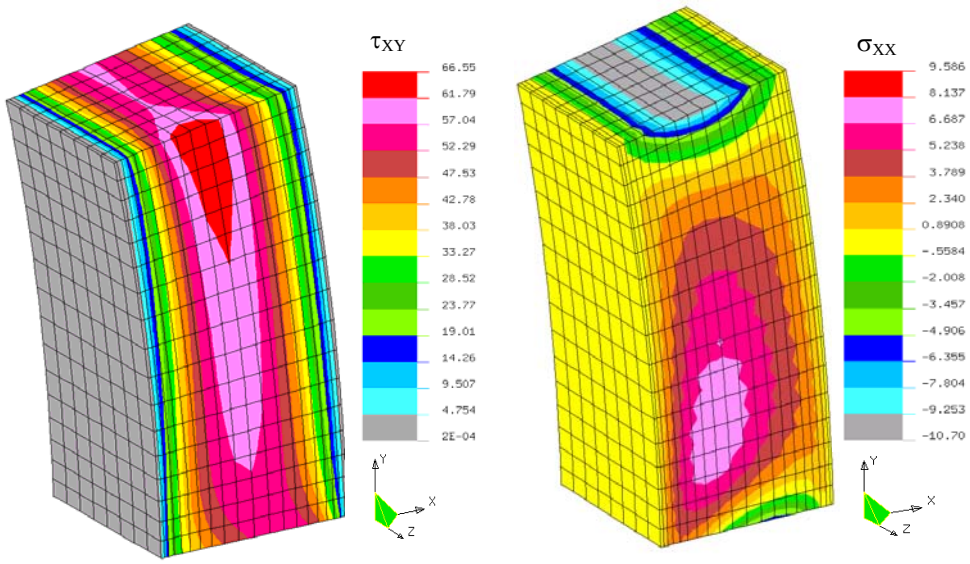

FIG. 6 — *Effect of beam curvature on the stress distribution according to 'Test B2' under 5.65 kN normal load (Solico BV)*

Effect of cross-sectional area — For test geometry C2 (thickness 15 mm and width 17 mm) and D (thickness 20 mm and width 30 mm), the respective stresses σ_{XX} and τ_{XY} are compared in Fig. 7. Fulfilling the requirements for a maximum shear stress of 58.8 MPa, a normal load of 20 kN should be applied on the C2 section and a normal load of 47 kN is applied on the D section. The stress distributions for both rectangular cross-sections are identical with a maximum shear stress of 65 MPa under the loading pin towards 58 MPa near the loading supports. Also compared to the stress distribution in small beam sections from Fig. 6, an identical stress distribution is calculated. Again the ASTM formula (1) is a small understatement of the maximum shear stress beneath the loading point, however it is a good estimation for the average shear stress over the beam length. Also the radial compressive stresses in Fig. 6 and Fig. 7 are nearly identical for different rectangular sections.

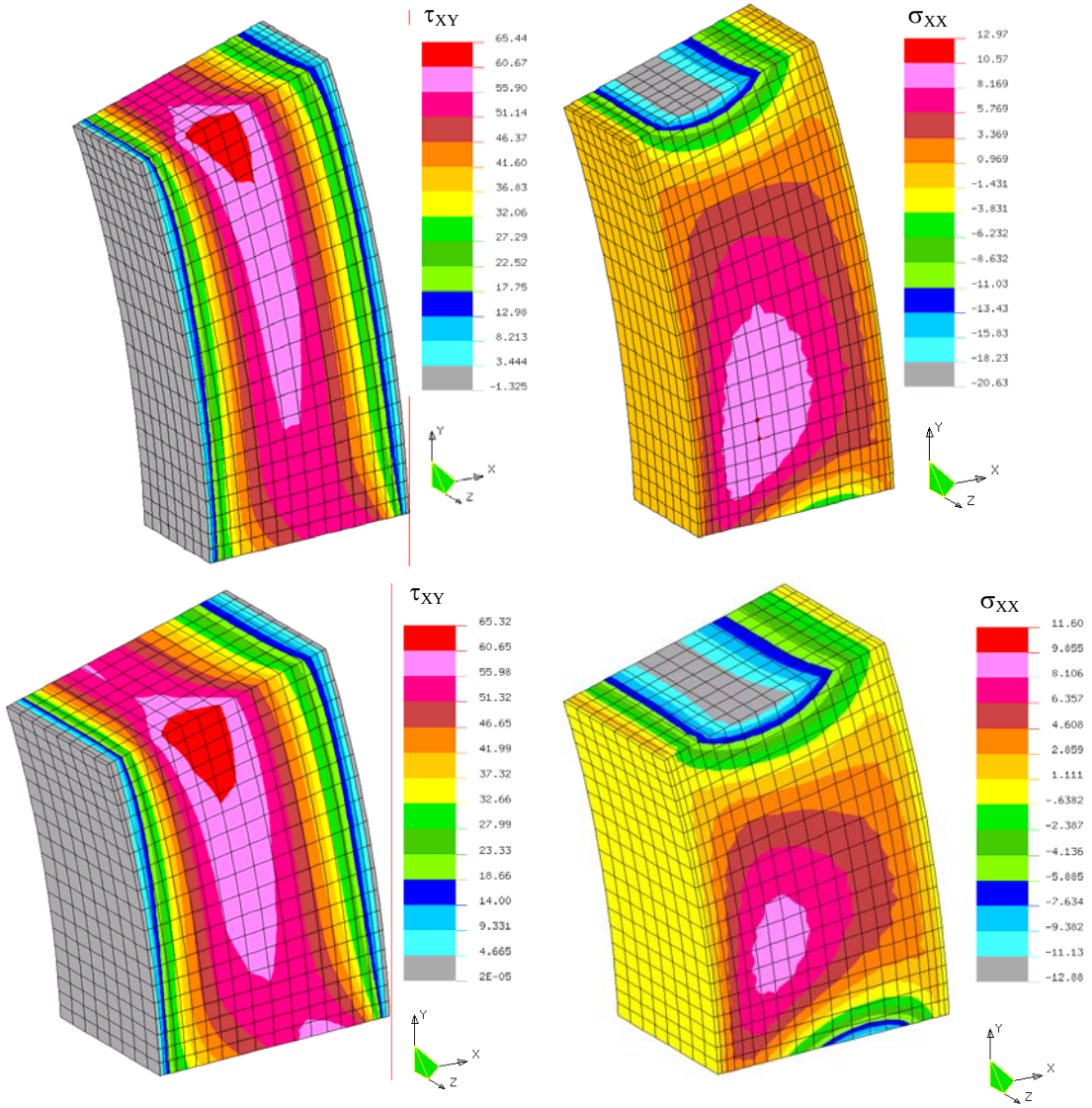

FIG. 7 — *Effect of cross-sectional area on the stress distribution according to 'Test C2' under 20 kN, upper, and 'Test D' under 47 kN, lower (Solico BV)*

Effect of convex or concave loading — A failure criterion for the maximum shear stress occurring under 45° relative to the loading direction, is evaluated on both a convex and a concave beam geometry as compared in Fig. 8, according to Test C1 and Test C2 under 20 kN normal load. The magnitude of the shear stresses in the centre of the beam is comparable, ranging between 50 MPa to 70 MPa, although it is more homogeneously distributed for a convex geometry than for a concave geometry. This is due to the larger span applied for good support. With the latter geometry, also stress concentrations near the loading point are minimised: in case of concave loading the maximum shear stress near the loading points rises towards 237 MPa, while it is about 165 MPa in case of convex loading. As the stress state near the loading points is of less interest in correlation to the full-scale tests, it is assumed that they should be minimised and that the bulk properties should dominate.

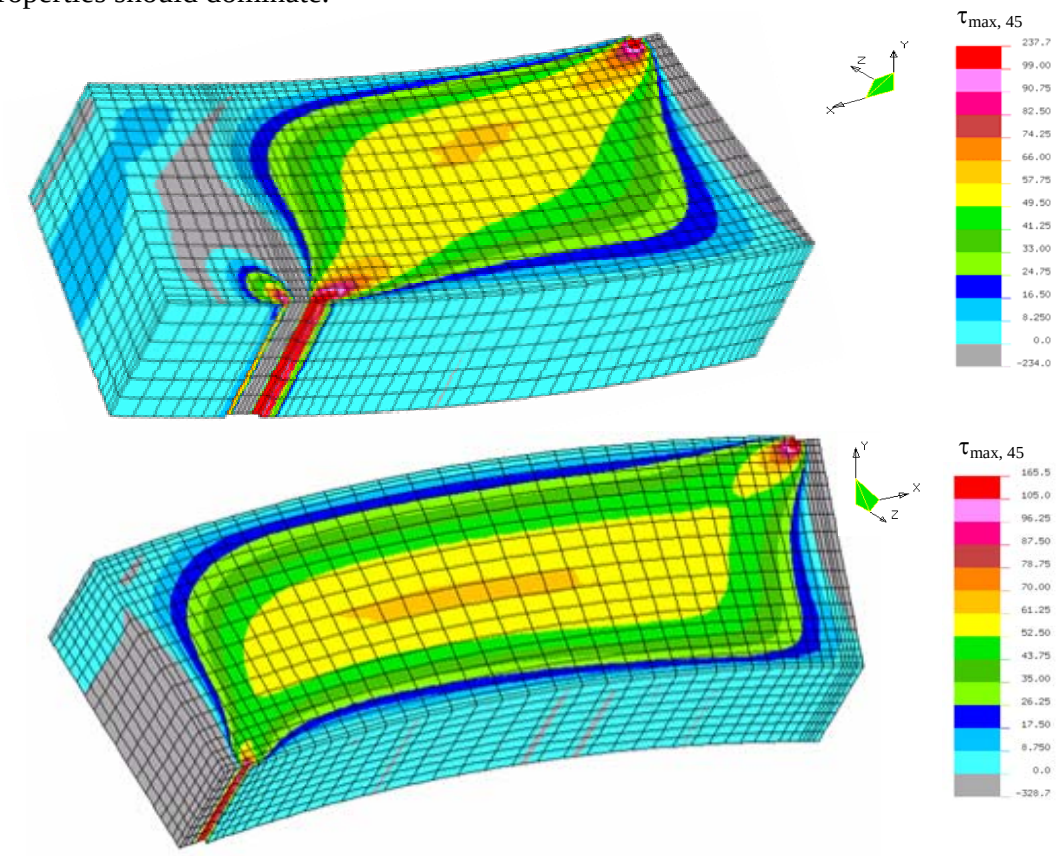

FIG. 8 — *Beam under concave loading according to 'Test C1' or convex loading according to 'Test C2' under 20 kN (Solico BV)*

A detail of the σ_{XX} and τ_{XY} stresses in the mid-section between support and load cylinder on a quarter of the CFR-E beam is calculated for a concave loaded beam (Test C1) in Fig. 9 and should be compared to the stress situation on a convex geometry (Test C2) previously calculated in Fig. 7. Under identical normal load of 20 kN, the shear stress under the pin attains a maximum of 58 MPa to 63 MPa for concave loading, while it is 60 MPa to 65 MPa in case of convex loading. It is also observed that a zone of 53 MPa to 58 MPa on a concave beam or 55 MPa to 60 MPa for a convex beam stretches over the

sample length and is more symmetric in case of convex loading. By comparing both convex and concave simulations, it seems that the convex geometry is more conservative for determination of a critical shear strength due to higher stresses in the bulk of the CFR-E ring and better symmetry.

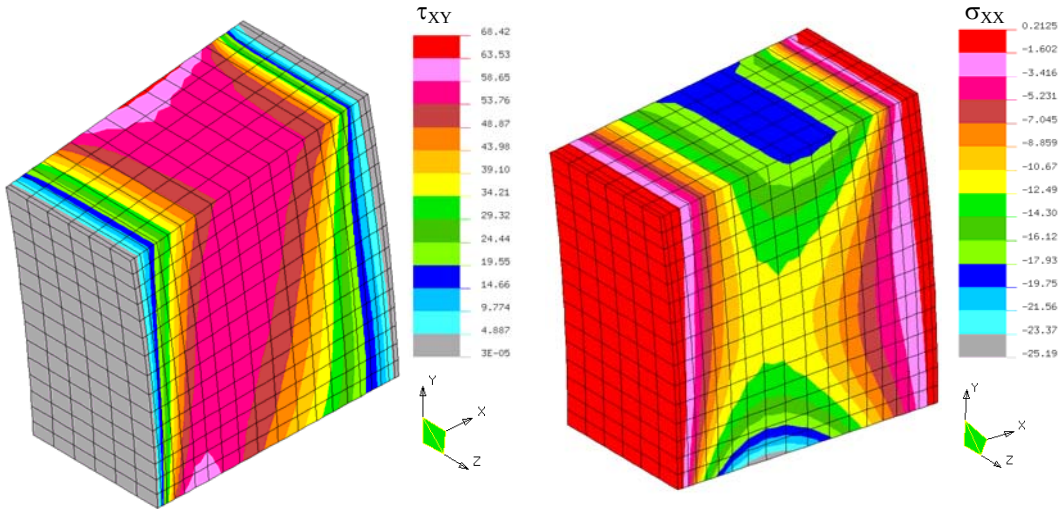

FIG. 9 — *Detailed stress distributions for a concave loaded beam according to 'Test C1' under 20 kN to be compared with Fig. 7 for convex beam (Solico BV)*

Effect of machined ring edges — As shown in Fig. 3 and according to the cross-section geometry for 'Test E', the real CFR-E ring is characterised by a round edge at the top with R = 5.7 mm and appropriate fillets in contact with the UHMWPE part of the bearing element (Fig. 1). Requiring the safety factor of 1.3 on the maximum full-scale shear stress of 45 MPa, a normal load of 37 kN should be applied on a cross section of 472 mm^2. The distribution of σ_{XY} and σ_{XX} stresses in a round edge CFR-E ring are calculated in Fig. 10 under 37 kN normal load, both in a longitudinal cut and a cut over the beam thickness. The shear stress in the centre of the beam is 57 to 63 MPa corresponding reasonably well to the ASTM estimation. From a thickness cut, it seems however that the shear stress is not symmetrically over the entire thickness and a detail of its maximum value shows that it attains 61 MPa. Near the machined edge, there is observed a gradual increase in stress over the circumference of the ring responsible for the asymmetric stress distribution. Radial-tangential shear stresses in the edge zone rise between 30 MPa to 45 MPa, corresponding to the reported maximum full-scale radial-axial shear stresses under non-hydrostatic state (Fig. 3). Also tensile stresses σ_{XX} accumulate near the round edge, varying between 1 and 5 MPa. These stresses were clearly not observed in previous rectangular sections, but appeared equally in the full-scale test.

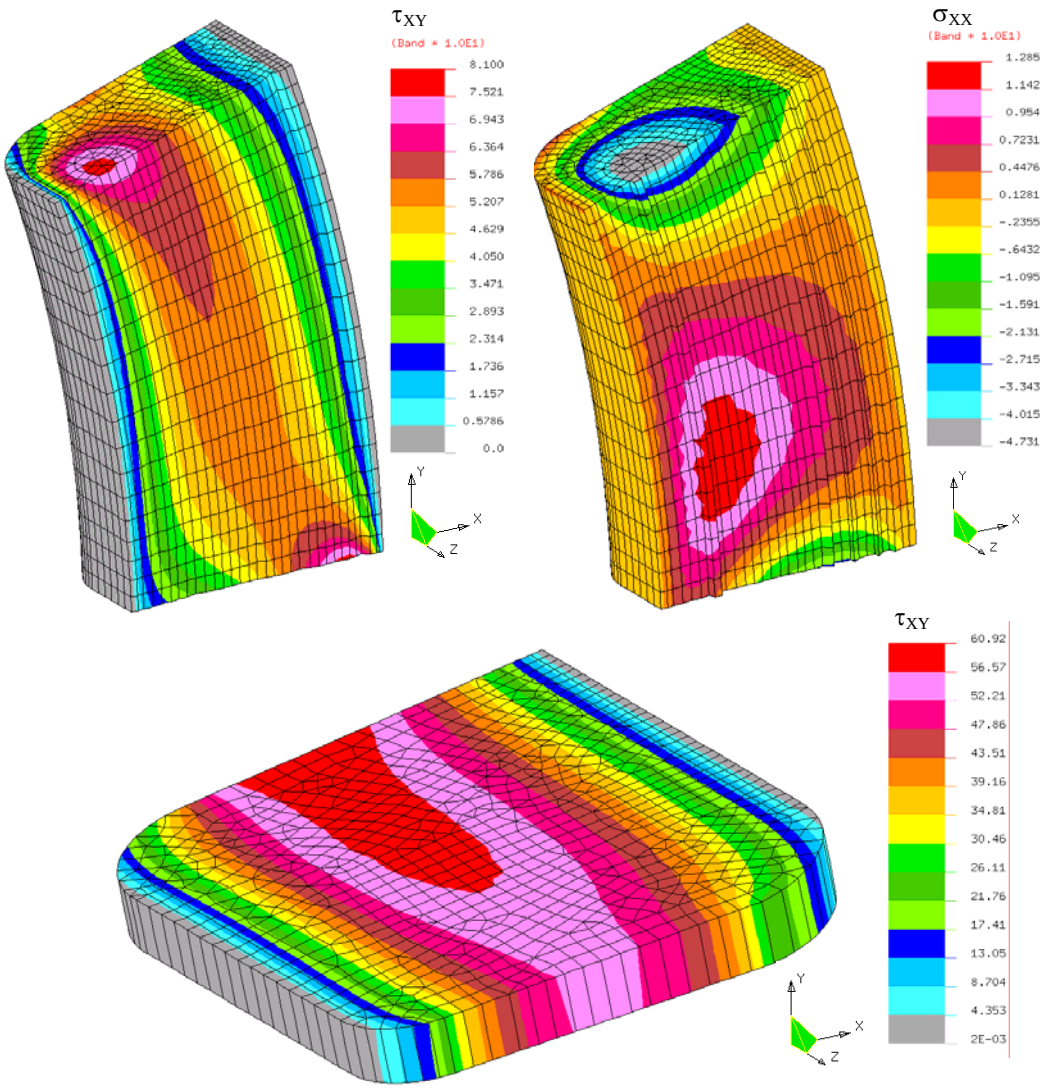

FIG. 10 — *Stress distributions for a CFR-E beam with machined edges* according to 'Test E' under 37 kN and a detailed thickness cut (Solico BV)

Experimental validation of Short-beam-shear tests

The stress-strain relationships for CFR-E rings of the same production quality but with different cross-section are plotted in Fig. 11, according to (i) Test A, (ii) Test D, (iii) Test E and (iv) Test B2. Multiple specimens are tested for one configuration, showing representative results. Possible differences in initial displacement at zero-load are attributed to the free space between the top surface of the beam and the pin during introduction of the normal load. By measuring accurately the different surface areas by means of a profilometer, it is verified that the shear stress at failure varies respectively (i) between 67 MPa to 69 MPa (12.7 kN to 12.8 kN) according to ASTM standards with cylinder supports, (ii) between 51 MPa to 54 MPa (32.7 kN to 34.6 kN) on rectangular section rings and (iii) between 48 MPa to 50 MPa (30.5 kN to 31.1 kN) on finished ring geometries. The Test B2 with different support and larger span compared to ASTM

standards (Test A) give lower strength. It is clear that a fit-to-purpose test on real sample geometries is presently required for evaluation of the machined CFR-E ring strength (Test E is called '*the Maeslant test*'), as standardised methods would imply an over-estimation of the shear strength capacity while eventual stress concentrations as modelled above are introduced on finished section rings, implying restrictions on the maximum shear strength. Concerning the discussion whether the ring segment should be loaded convexly or concavely, it is verified that the concave geometry in Test C1 provides an ILSS that is 1.4 times higher than the convex geometry in Test C2.

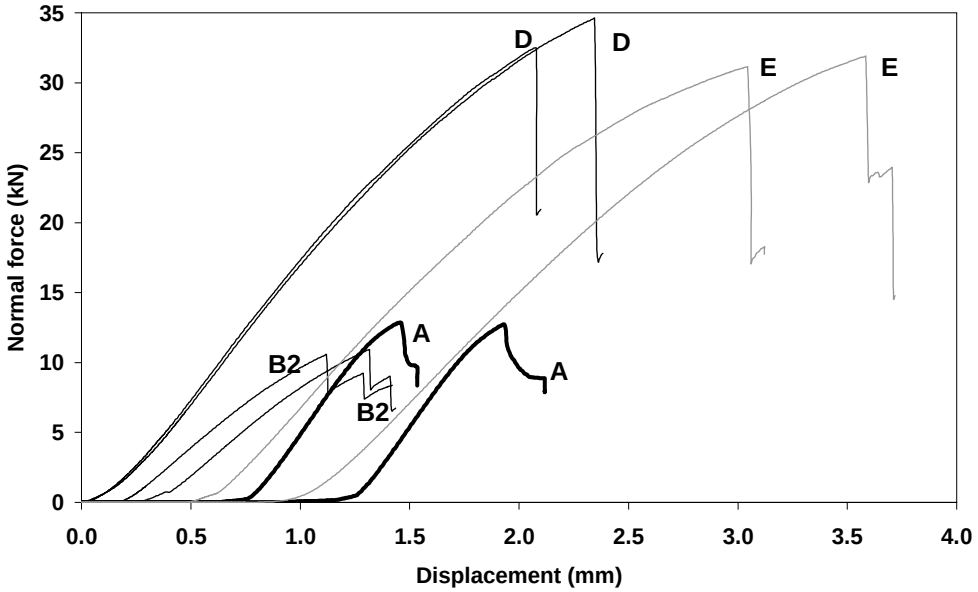

FIG. 11 — *Experimental stress-strain curve for Short-beam-shear tests of different ring geometries with indication of test numbers according to definitions in Fig. 2*

As it is observed in Fig. 11 a critical normal load of 37 kN for a 'Test E' as initially assumed, is practically not attained, although improvements in filament winding conditions [10] and composite composition (fibre content and porosity) [9] were considered. However, it was experimentally verified that a CFR-E ring with critical normal load of 20 kN during short-beam-shear testing not induced full-scale fracture at 180 MPa contact pressure. According to previous safety factor of 1.3, a normal load of 27 kN should then be required for representative small-scale testing with a global safety factor of at least 1.3*180/150 = 1.47 on shear failure. Taking into account the machining tolerances on the CFR-E ring diameters for determination of the cross section area, the effective shear stress under 20, 27 and 37 kN normal loads are given in Table 1. As the rings are processed by filament winding on a rotating mandrel with well-known diameter, variations in inner diameter are negotiated. A machining operation on the outer diameter of the CFR-E ring possibly causes a tolerance on the outer ring diameter between 248.50 and 249.50 mm. The nominal diameter of the final ring is 249.00 mm with 453 mm^2 cross-section area. More details about the influence of machining tolerances on the deformation and stiffness of the polymer bearing elements were experimentally studied in Ref. [11]. From Table 1, it seems that a critical normal load of 27 kN coincides with an

ILSS of 45 MPa, which is representative for the full-scale shear stress of 33 MPa (Fig. 3) calculated at the outer diameter where cracks initiate, with safety factor 1.3. An ILSS of 58.8 MPa as initially modeled is too conservative in relation to full-scale tests.

TABLE 1 — Influence of the cross section after machining of the CFR-E ring on calculated ILSS under 20, 27 and 37 kN normal load in a short-beam-shear 'Test E'

Inner diameter (mm)	Outer diameter (mm)	Cross-section area (mm^2)	ILSS (MPa) at 20 kN normal load	ILSS (MPa) at 27 kN normal load	ILSS (MPa) at 37 kN normal load
209.0	248.50	447	33.5	45.3	62.1
209.0	249.00	453	33.1	44.7	61.2
209.0	249.50	472	31.8	42.9	58.8

From the macrographs in Fig. 12 it is verified that each ring failed under maximum normal load in shear mode (no fibre fracture due to high tensile hoop stress observed), and additional fracture near the machined edge is observed for the 'Test E' specimen. This fracture pattern corresponds well to the stresses calculated in Fig. 10.

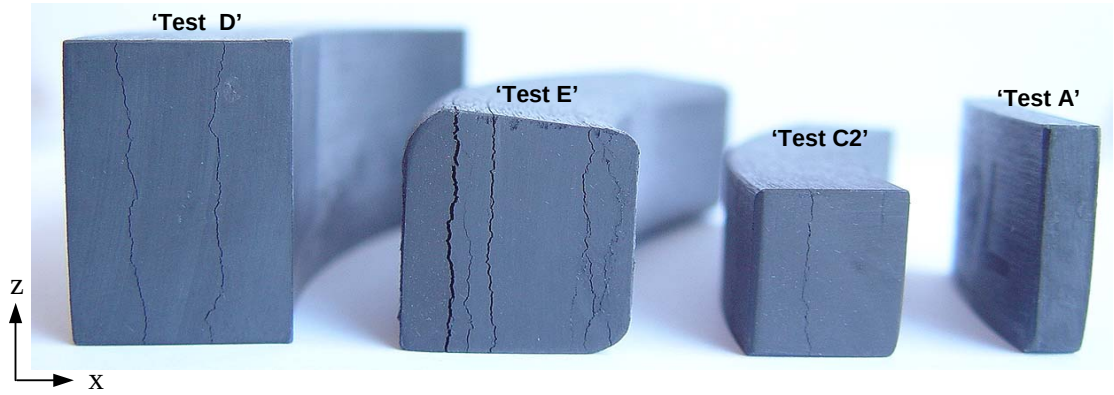

FIG. 12 — *Failure mode of CFR-E rings with different cross section after Short-beam-shear test*

Discussion and Conclusions

Present study originates from failure observed on full-scale tested carbon fibre / epoxy composite components. Performing large-scale tests is however time-consuming and expensive as a qualification test, although the most reliable. The problem in scaling test results from laboratory equipment towards a real construction is universal and should be conducted with care [12]. A first approximation of small-scale behaviour is based on testing standards, very useful for a relative selection of construction materials depending on their strength, friction, wear, etc. They allow inter-laboratorial compatibility and make literature surveys easy. As presently demonstrated, however, those tests are difficult to be uniquely correlated to the in-situ performance and often give an over-estimation of the material's behaviour. Main problems in small-scale testing are a good simulation of boundary conditions and stress concentrations as close as possible to the real

construction. In this respect, the effect of stress concentrations depending on different test geometries and supporting methods for a standardised short-beam-shear test are studied by means of finite element calculations. It seems that the stress distribution symmetry strongly depends on the sample cross-section, the loading supports and the loading type. In addition to the standardised beam geometry, a specific stress distribution is introduced over the machined edge of the beam. It is mainly the latter that was important in full-scale testing, as a non-hydrostatic stress component was responsible for lower shear resistance compared to the bulk of the carbon composite ring.

For present design of polymer bearing reinforcements, a small-scale selection criterion is determined on a real sample geometry, requiring a normal load of 27 kN on a short-beam-shear test and attaining a representative state of stress in both small-scale and full-scale test samples. The final implementation of the polymer bearing elements as sliding surface in a heavily loaded ball-joint approved present design philosophy, as failure was successfully avoided after small-scale qualification of the composite ring.

References

[1] Kedward, K.T., "On the short beam test method", *Fibre Science and Technology* 5 (1972), pp. 85-95

[2] Sawyer, J.W., "Investigation of test technique for measuring shear strength of two-dimensional carbon-carbon composites", NASA Report No. TM 100647 (1988)

[3] Samyn, P., De Baets, P., Van Paepegem, W., Van Schepdael, L., Suister, E., Leendertz, J.S., "Design of a carbon/epoxy reinforcing ring reducing creep of UHMWPE in high-loaded sliding contacts", *Proceedings on 8th International Conference on Tribology*, Veszprem (Hungary) 2004, pp. 89-96.

[4] Leendertz, J.S., Van Schepdael, L., Van Paepegem, W., Samyn, P., De Baets, P., Degriek, J., "Modification of the ball bearing of the storm surge barrier near Rotterdam (Nl)", submitted to *Stahlbau* (2005)

[5] Liu, H.S., Liao, W.C., Tseng, L., Lee, W.H., Sawada, Y., "Compression strength of pre-damaged concrete cylinders reinforced by non-adhesive filament wound composites", *Composites* Part A 35 (2004), pp. 281-292

[6] Samyn, P., Van Schepdael, L., Leendertz, J.S., Gerber, A., Van Paepegem, W., De Baets, P., Degrieck, J., "Large-scale friction and wear tests on a hybrid UHMWPE-pad / Primer Coating combination used as bearing element in an extremely high-loaded ball-joint", *Tribology International 2005*. (in press).

[7] Hine, P., Duckett, R.A., Kaddour, A.S., Hinton, M.J., Wells, G.M., "The effect of hydrostatic pressure on the mechanical properties of glass fibre/epoxy unidirectional composites", *Composites* Part A 36 (2005), pp. 279-289

[8] Pahr, D.H., Rammerstorfer, F.G., Rozenkrans, P., Humer, K., Weber, H.W., "A study of short-beam-shear and double lap shear specimens of glass fabric/epoxy composites", *Composites* Part B 33 (2002), pp. 125-132

[9] Samyn, P., Van Schepdael, L., Leendertz, J.S., Van Paepegem, W., De Baets, P., Degrieck, J., "Fracture assessment of carbon fibre / epoxy reinforcing rings through a combination of full-scale testing, small-scale testing and stress modelling", submitted to *Engineering Failure Mechanics* (2005)

[10] Cohen, D., "Influence of filament winding parameters in composite vessel quality and strength", *Composites* Part A 28 (1997), pp. 1035-1047

[11] Samyn, P., Van Schepdael, L., Leendertz, J.S., Van Paepegem, W., De Baets, P., Degrieck,

J., “Deformation of reinforced polymer bearing elements on full-scale compressive strength and creep tests under yielding conditions”, submitted to *Polymer Testing* (2005)

[12] Samyn, P., De Baets, P., “Friction and wear of acetal: a matter of scale”, *Wear*, 259 No. 1-6 (2005), pp. 697-702

Acknowledgements

The authors of Ghent University appreciate the cooperation with the Nederlandse Rijkswaterstaat for manufacturing of test specimen and to be involved in the re-design of the Maeslant storm surge barrier. Solico BV is greatly acknowledged for the performance of finite element modelling and allowance to publish test results. Many thanks to Ludo and Han for their help and useful discussions!